

3D Printing of Anode Architectures for Customized Lithium-Ion Batteries

U. Rist^a, F. Ball^a, W. Pfleging^a

^aKarlsruhe Institute of Technology, IAM-AWP, P.O. Box 3640, 76021 Karlsruhe, Germany

ABSTRACT

The expansion of renewable energies is increasing the demand for affordable and enhanced energy storage systems. Here, 3D lithium-ion battery concepts represent a promising approach to improve e.g., energy and power density as well as lifetime of batteries. This work explores the potential of the laser induced forward transfer (LIFT) method as a tool for the realization of new types of 3D electrode architectures on structural and compositional level. Using a pulsed nanosecond UV laser, several parameters were examined to determine the variables affecting reliable material and voxel transfer, including laser fluence as a function of donor layer thickness and donor paste-to-substrate distances, as well as the influence of viscosity and solid content of the anode paste. In addition, a 3D anode is produced by combining laser structuring with subsequent localized laser printing with silicon-rich anode paste.

Keywords: LIFT, printing anodes, ablation, lithium-ion battery, 3D battery, multilayer anode, silicon, graphite

1. INTRODUCTION

With regard to the expansion of renewable energies and the increasing electrification of transport, the demand for affordable and improved energy storage systems is growing. Here, 3D lithium-ion battery concepts represent a promising approach to enhance the electrochemical performance of battery cells. Novel electrode concepts can increase the energy and power density, cycle stability, fast charging capability, and lifetime compared to the state-of-the-art battery [1–3]. Current research focuses on patterned electrodes [4, 5] and multilayer electrodes [6, 7] with graphite and silicon. Here, silicon would offer an order of magnitude higher specific capacity in comparison to graphite [8]. During lithiation silicon undergoes a huge volume expansion of up to 300 % which leads to capacity loss and a shortened lifetime [9]. A 3D architecture of the silicon electrode can reduce the mechanical stress on the layer by creating space for volume expansion [5, 10]. In addition to the generation of 3D architectures with laser structuring the laser induced forward transfer (LIFT) process offers a versatile and reliable tool for creating customized architectures [7, 11]. In recent studies LIFT was used to print micro-batteries [12], unstructured anodes for coin cells [7] and subsequently structured cathodes [13]. In the current investigations on the optimization of the printing process, the behavior of the LIFT process with anode pastes, also called anode inks, is examined in detail. Therefore, the impact on the laser fluence which is needed for a transfer, in the following also referred to as threshold fluence, is investigated for anode inks with different properties. The viscosity and the solid content are varied by using binders with different molecular weight and respective chain lengths, while keeping the solid content and different binder concentrations in the solution. In addition to varying the anode ink properties, the layer thickness of the anode ink on the donor plate and the distances between the anode paste and the substrate are also modified. As binder for the paste polyacrylic acid (PAA) is used in contrast to prior studies which employed PVDF [7, 12–16]. In addition, by combining subtractive and additive laser techniques, a customized architecture is developed in which an anode layer is patterned and subsequently a silicon-rich paste is printed into the structures.

*ulrich.rist@kit.edu; phone: +49 721 608 28161

2. EXPERIMENTAL SET-UP

Figure 1 shows a schematic view of the setup of the LIFT process. A frequency tripled Nd:YAG laser (Lumentum, USA, Model: Q301-HD-1000R) with an operational wavelength of 355 nm, a pulse width of 78 ns, a maximum power of 10 W, and a maximum repetitions rate of 30 kHz is used. A diffractive optical element (DOE) is applied to transform the gaussian laser intensity profile to a top-hat one. With the mask selector followed by the DOE the laser geometry can be changed to smaller circles and rectangles by shadowing the remaining laser beam. For the studies no aperture is used, so the geometry of the beam is a rectangle with a side length of 175 μm and for the printing with silicon a rectangle aperture with a side length of 47 μm is used. After the mask selector an objective lens with a demagnification factor of 3.5 focuses the laser beam onto the backside of the anode paste. The anode paste is coated on a quartz glass wafer (DSP-200 \times 0675-SGQ-00, Wafer Universe, Germany) with a diameter of 200 mm and a thickness of 0.675 mm, in the following also called donor plate. The substrate on which the anode paste is printed is a 9 μm thick copper foil.

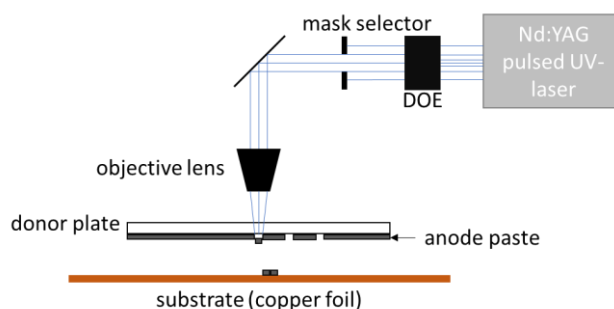


Figure 1: Schematic representation of the used setup for the LIFT process.

The anode paste used for printing contains 85 wt.% flake-like graphite (T808, Targray, Canada) with an average particle size of $d_{50} = 4.9 \mu\text{m}$, measured by laser scattering. To increase the electric conductivity of the electrode, the paste contains 5 wt.% carbon black (Super C65, Timcal, Swiss). As binder 10 wt.% PAA (181285/306215/306223, Merck, Deutschland) with different chain length (molecular weight: 450 kg mol⁻¹, 1.25 Mg mol⁻¹ and 3 Mg mol⁻¹) are used. The binders are solved in a 1:1 solution of deionized water and glycerol (99.5 %, Thermo Scientific, USA). The glycerol is used to increase the drying time of the anode ink and thus increase the process window. The silicon paste, which is used for the customized architecture contains 40 wt.% silicon (SI-15008, Targray, Canada, $d_{50} = 72 \text{ nm}$). 40 wt.% carbon black is added and as binder 20 wt.% PAA with a molecular weight of 450 kg mol⁻¹ is used. The solvent is a 1:1 solution of deionized water and glycerol. The electrode layer used as base layer for the customized architecture is based on the recipe by Kumberg et. al. [17] and contains 93 wt.% T808, 1.4 wt.% carbon black, and as binders 1.87 wt.% sodium carboxymethyl cellulose and with 3.73 wt.% styrene-butadiene rubber, and deionized water as solvent.

The anode printing was according to the LIFT process described by Fernández-Pradas [18] for printing fluids. The LIFT process of fluids works with a partial evaporation of the paste and the expansion of the evaporated gas causes a transfer of a voxel to the substrate. The anode paste is coated onto the quartz glass wafer with a doctor blade. The layer thickness of the graphite inks is set at 40 μm , with the exception to study the impact of the layer thickness.

3. RESULTS & DISCUSSION

LIFT process studies

The LIFT process of transferring fluids has already been investigated with, e.g. silver nanoparticle ink [19–23] and a water and glycerol solvent with additives [24–26]. For the study presented here, the threshold fluence is investigated as a function of various properties. The experiments are always performed with a freshly coated donor plate, since the viscosity of the anode ink on the donor plate changes over time. The LIFT process is started about 10 min after coating. In each process, lines with a length of 2 mm and a point-to-point distance of 0.5 mm are printed, so every single transferred voxel is visible separately. In Figure 2 from the beginning of a column to the end the laser fluence is increased from 0.16 J cm⁻² up to 1.57 J cm⁻² with a step width of 0.049 J cm⁻². This process is repeated for different distances between the anode layer on

the donor plate and the copper foil, ranging from 125 μm up to 200 μm . The first line with all transferred voxels visible is assigned as the threshold fluence. All studies in this paper are designed according to the principle described and illustrated by an example in Figure 2.

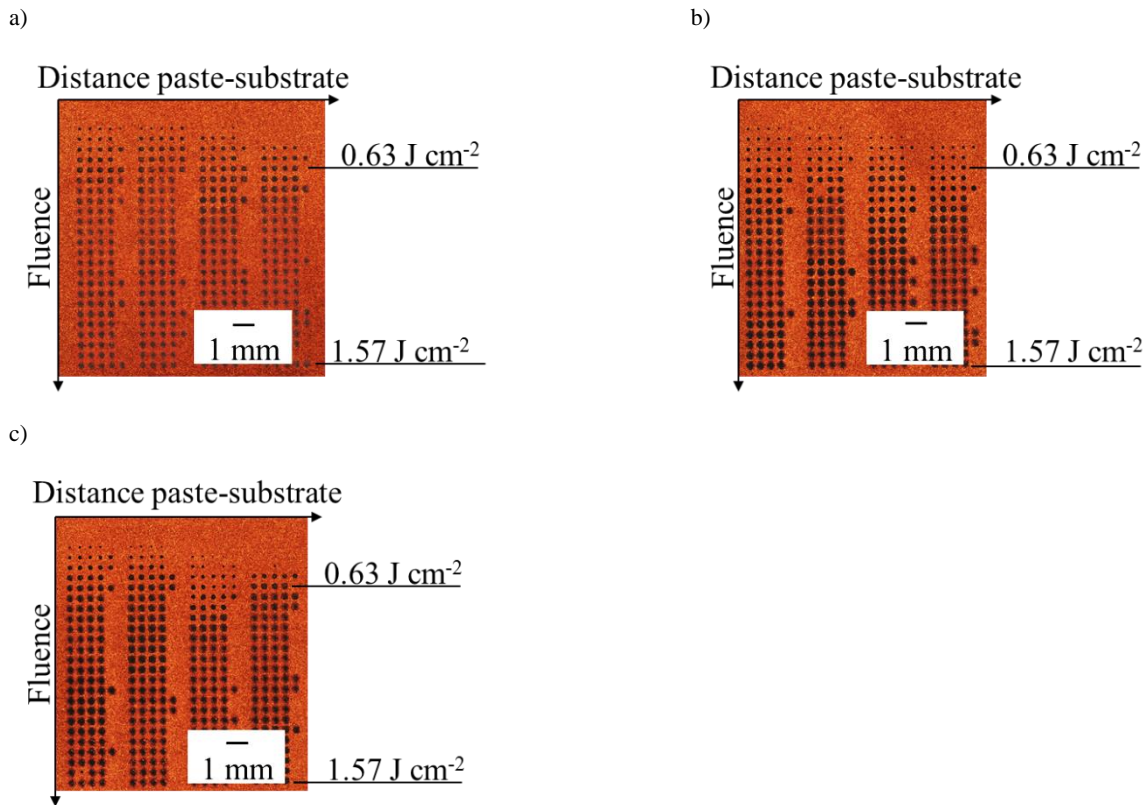


Figure 2: Printings made for the investigation of the dependence of the threshold fluence in comparison to the viscosity of the pastes at different distances between anode paste and copper foil. The fluence ranging from 0.16 J cm^{-2} to 1.57 J cm^{-2} with a step width of 0.049 J cm^{-2} . The paste to substrate distance ranging from 125 μm up to 200 μm . The used solution has a binder concentration of 5 wt.%. Viscosity: a) PAA 450k: 1.8 Pa s, b) PAA 1.25M: 6.5 Pa s, c) PAA 3M: 8.8 Pa s.

In Figure 3, the results which are shown in Figure 2 are displayed.

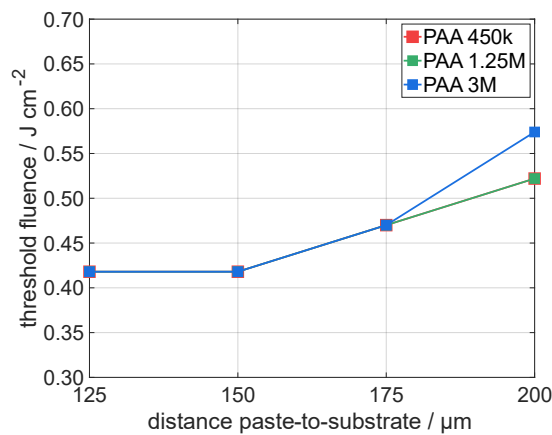


Figure 3: Threshold fluence depending on the distance between anode paste and copper foil. All anode inks have the same composition, but due to the usage of PAAs with different molecular weights, different viscosities are achieved. The solution used has a binder concentration of 5 wt.%. Viscosity: PAA 450k: 1.8 Pa s; PAA 1.25M: 6.5 Pa s; PAA 3M: 8.8 Pa s. Lines are guides to the eye.

For the three binders for the paste-to-substrate distances of 125 μm and 150 μm no change in the threshold fluence (0.42 J cm^{-2}) for a transfer is observed (Figure 3). At larger distances an increase of the threshold fluence is detected. The anode paste with the binder with the highest chain length and the highest viscosity exhibits a slightly higher increase at a paste-to-substrate distance of 200 μm compared to the other anode inks.

Further the impact of the thickness of the anode layer on the threshold fluence is analyzed (Figure 4).

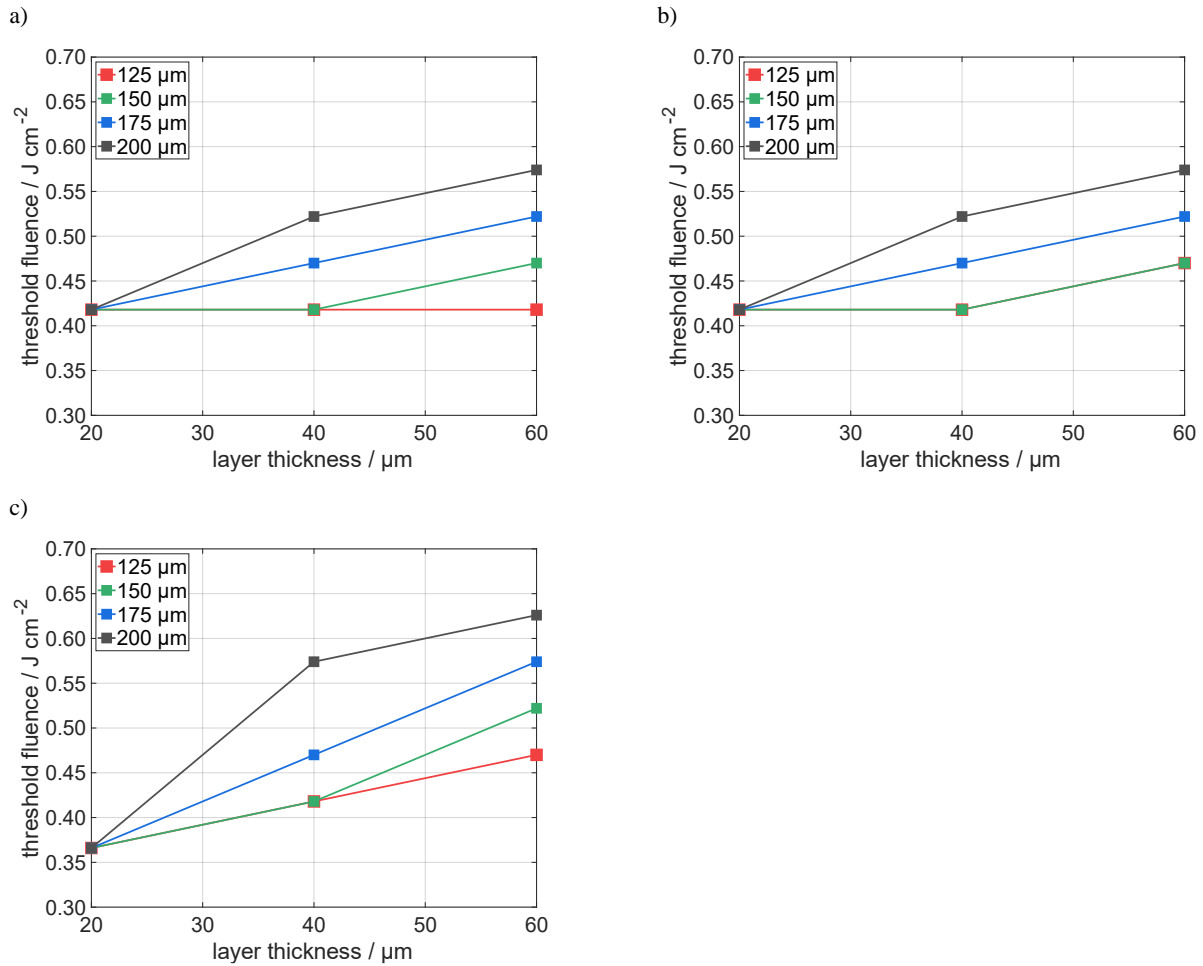


Figure 4: Threshold fluence depending on the anode paste layer thickness on the donor plate. All anode inks have the same composition, but PAAs with different molecular weights are used. The solution used has binder concentration of 5 wt.%. a) PAA 450k, b) PAA 1.25M and c) PAA 3M. Lines are guides to the eye.

In Figure 4a), the results of the material transfer studies of the paste with PAA 450k is displayed. For an anode paste layer thickness of 20 μm all paste-to-substrate distances have the same threshold fluence. With increasing the anode paste layer thickness for the gap width of 175 μm and 200 μm the threshold fluence increases. For the gap width of 150 μm an increase in the threshold fluence appears only at the anode paste layer thickness of 60 μm . The threshold fluence stays the same for all solid contents for the gap width of 125 μm . The results for the paste with PAA 1.25M are displayed in Figure 4b). Only the threshold fluence at a gap width of 125 μm and an anode paste layer thickness of 60 μm increases compared to Figure 4a). For the paste with PAA 3M, displayed in Figure 4c), there are clear differences relative to the other binders. Here, the threshold fluence for the transfer of 60 μm anode paste layer thickness at 150 μm , 175 μm and 200 μm gap widths as well as for the 40 μm layer at 200 μm distance is higher than for the pastes with lower viscosity. On the other hand, the transfer at 20 μm anode paste layer thickness is lower than for the other pastes. Regarding the diagrams of Figure 4, it can be said that with increasing anode paste layer thickness the threshold fluence increases.

In addition to the anode paste layer thickness the viscosity can have an impact on the threshold fluence. Therefore, as described earlier, different binders with different chain lengths are used, leading to different viscosities. The composition of the solid and fluid content is the same for each paste.

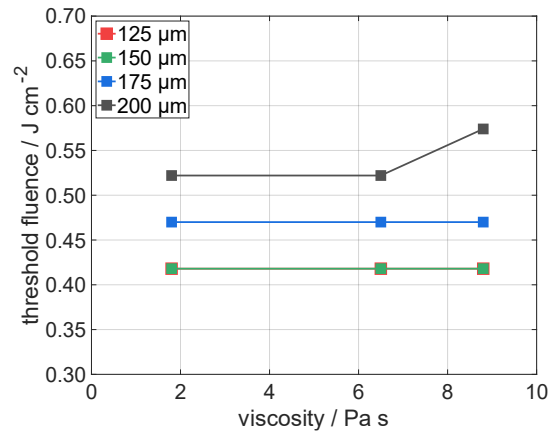


Figure 5: Threshold fluence depending on the viscosity of the paste. To vary the viscosity, binders with different molecular weight are used, PAA 450k, PAA 1.25M and PAA 3M. The solid and the fluid content are the same for each viscosity. Lines are guides to the eye.

For the distance between donor plate and anode paste of 125 μm and 150 μm, the same threshold fluence of 0.42 J cm⁻² is achieved for each viscosity (Figure 5). For the gap width of 175 μm the threshold fluence is the same for each viscosity, 0.47 J cm⁻², but higher than for the smaller distances. The threshold fluence of the 200 μm gap width is higher than for the smaller ones and here an increase at the highest viscosities can be observed. For the applied viscosity range and gap widths, the threshold fluence is almost independent of the viscosity, and only at the highest distance and viscosity a slightly increased threshold fluence is detected.

The impact of the fluid content in the paste is investigated. For this purpose, the binder PAA 450k is used for all measurements and the solid content of the ink solutions with different binder concentrations are studied. The composition of the solid content is the same for each paste used for this investigation.

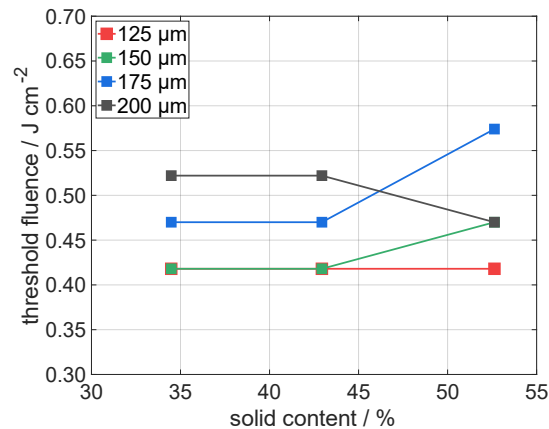


Figure 6: Threshold fluence depending on the solid content of the anode paste for different paste-to-substrate distances. PAA 450k is used as binder and the binder concentration in the solution is changed from 5 wt.% over 7 wt.% up to 10 wt.%. The change in solids content leads to viscosity values of 1.8 Pa s over 7.4 Pa s up to 30.6 Pa s. The composition of the solid content is the same, only the amount of solvent in the paste is changed. Lines are guides to the eye.

With a gap width of 125 μm, the threshold fluence remains the same and is not affected by the solids content of the paste (Figure 6). At 150 μm, the same threshold fluence as at 125 μm is detected, except for the highest solid content, where the value increases. The threshold fluence values for 175 μm gap width are higher than for smaller ones and show only a dependence of the threshold fluence on the highest studied solid content. At a gap width of 200 μm the decreasing threshold

fluence at the highest solid content seems to be an exception when comparing to the behavior at smaller gap widths. The exception can be explained by the particle size, which is at least one order of magnitude larger than in most other studies, e.g., the studies with silver nanoparticles [19–23]. The increased particle size may cause a dispersion in the threshold fluence. The increase of the threshold fluence at the highest solid content and so the highest viscosity is in good agreement with the results shown in Figure 5. The anode ink with the highest solid content has an almost 3.5 times higher viscosity, 30.6 Pa s compared to 8.8 Pa s. The higher threshold fluence for higher gap widths can therefore also be explained by the higher viscosity of the anode paste, or it could be a superposition of the effects of viscosity and solid content. Further studies are needed to separate the impact of the viscosity and the impact of the solid content, whereas it seems that the impact is small compared to the impact of the gap width and the paste thickness.

Customized anode architecture

As a customized anode architecture, an anode layer with graphite as active material is laser structured. Subsequently a silicon rich anode paste is printed in the generated structures to increase the capacity of the electrode. An example of the achieved electrode architecture is shown in Figure 7.

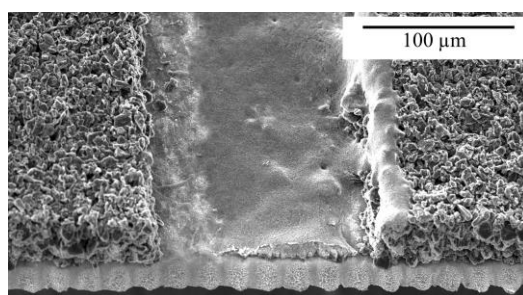


Figure 7: SEM picture of a customized battery architecture achieved by structuring a graphite anode layer and subsequently printing by LIFT in the generated structures with a silicon rich paste.

The line structure in graphite anode is obtained by fs laser ablation. The lines have each a width of 100 μm . After patterning the silicon rich slurry is printed into the generated line structures. A rectangular aperture with a side length of 47 μm is used. Because of the huge volume expansion during lithiation, only a thin silicon layer is printed into the cavities.

4. CONCLUSION & OUTLOOK

In this study, the impact of the properties of anode inks used in a LIFT process and related properties of the process was investigated. The influence of the distance between donor plate and substrate, the anode paste layer thickness, the ink viscosity, and the solid content of the ink were examined. The gap width between the donor plate and the substrate showed an impact on the threshold fluence. With increasing distances, the threshold fluence increased. Increasing the thickness of the anode ink on the donor plate led to an increased threshold fluence. For the investigation of the dependence on the viscosity, binders with different molecular weight were used while keeping the solid and fluid content at a constant level. It was shown that the ink viscosity has a small influence on the threshold fluence only at higher gap widths and higher viscosities. The change in solid content showed the same influence on the threshold fluence as the ink viscosity. A further investigation of the impact of the solid content without a change of viscosity is required. A new customized electrode architecture was successfully realized, where an anode layer with graphite as active material was structured with lines widths of 100 μm and subsequently a silicon-rich ink was printed into the cavities. In ongoing studies, the electrochemical characterization of the customized battery layer cells will be performed. In addition, a further optimization of the printing process as function of structure geometry is necessary regarding the amount silicon and respective ink composition.

REFERENCES

- [1] W. Pfleging, *Int. J. Extrem. Manuf.* **2021**, 3 (1), 12002. DOI: 10.1088/2631-7990/abca84.
- [2] A. Meyer, F. Ball, W. Pfleging, *Nanomaterials (Basel, Switzerland)* **2021**, 11 (12). DOI: 10.3390/nano11123448.

- [3] J. B. Habedank, J. Endres, P. Schmitz, M. F. Zaeh, H. P. Huber, *Journal of Laser Applications* **2018**, *30* (3), 32205. DOI: 10.2351/1.5040611.
- [4] J. Park, C. Jeon, W. Kim, S.-J. Bong, S. Jeong, H.-J. Kim, *Journal of Power Sources* **2021**, *482*, 228948. DOI: 10.1016/j.jpowsour.2020.228948.
- [5] W. Pflöging, P. Gotcu, P. Smyrek, Y. Zheng, J. K. Lee, H. J. Seifert, in *Laser Micro-Nano-Manufacturing and 3D Microprinting*, Vol. 309, Springer Series in Materials Science (Eds: A. Hu), Springer International Publishing. Cham **2020**. DOI: 10.1007/978-3-030-59313-1_11.
- [6] L. Ji, H. Zheng, A. Ismach, Z. Tan, S. Xun, E. Lin, V. Battaglia, V. Srinivasan, Y. Zhang, *Nano Energy* **2012**, *1* (1), 164 – 171. DOI: 10.1016/j.nanoen.2011.08.003.
- [7] U. Rist, A. Reif, W. Pflöging, in *Laser-based Micro- and Nanoprocessing XVI* (Eds: R. Kling, A. Watanabe), SPIE **2022 - 2022**. DOI: 10.1117/12.2609588.
- [8] A. Baasner, F. Reuter, M. Seidel, A. Krause, E. Pflug, P. Härtel, S. Dörfler, T. Abendroth, H. Althues, S. Kaskel, *J. Electrochem. Soc.* **2020**, *167* (2), 20516. DOI: 10.1149/1945-7111/ab68d7.
- [9] W. Pflöging, *Nanophotonics* **2018**, *7* (3), 549 – 573. DOI: 10.1515/nanoph-2017-0044.
- [10] Y. Zheng, H. J. Seifert, H. Shi, Y. Zhang, C. Kübel, W. Pflöging, *Electrochimica Acta* **2019**, *317*, 502 – 508. DOI: 10.1016/j.electacta.2019.05.064.
- [11] D. Moldovan, J. Choi, Y. Choo, W.-S. Kim, Y. Hwa, *Nano convergence* **2021**, *8* (1), 23. DOI: 10.1186/s40580-021-00271-w.
- [12] H. Kim, T. E. Sutto, J. Proell, R. Kohler, W. Pflöging, A. Piqué, in *Laser-based Micro- and Nanoprocessing VIII*, SPIE Proceedings (Eds: U. Klotzbach, K. Washio, C. B. Arnold), SPIE **2014**. DOI: 10.1117/12.2037287.
- [13] P. Smyrek, H. Kim, Y. Zheng, H. J. Seifert, A. Piqué, W. Pflöging, in *Laser 3D Manufacturing III*, SPIE Proceedings (Eds: B. Gu, H. Helvajian, A. Piqué), SPIE **2016**. DOI: 10.1117/12.2211546.
- [14] A. Piqué, C. B. Arnold, H. Kim, M. Ollinger, T. E. Sutto, *Appl. Phys. A* **2004**, *79* (4-6), 783 – 786. DOI: 10.1007/s00339-004-2586-1.
- [15] T. E. Sutto, M. Ollinger, H. Kim, C. B. Arnold, A. Pique, *Electrochemical and Solid-State Letters* **2006**, *9* (2), A69-A71. DOI: 10.1149/1.2142158.
- [16] R. Wartena, A. E. Curtright, C. B. Arnold, A. Piqué, K. E. Swider-Lyons, *Journal of Power Sources* **2004**, *126* (1-2), 193 – 202. DOI: 10.1016/j.jpowsour.2003.08.019.
- [17] J. Kumberg, M. Müller, R. Diehm, S. Spiegel, C. Wachsmann, W. Bauer, P. Scharfer, W. Schabel, *Energy Technol.* **2019**, *7* (11), 1900722. DOI: 10.1002/ente.201900722.
- [18] Juan M. Fernández-Pradas, in *Laser Printing of Functional Materials: Electronics, 3D Microfabrication and Biomedicine* (Eds: A. Piqué, P. Serra), John Wiley & Sons Incorporated. Newark **2018**.
- [19] R. C. Y. Auyeung, H. Kim, S. Mathews, A. Piqué, *Optics express* **2015**, *23* (1), 422 – 430. DOI: 10.1364/OE.23.000422.
- [20] L. Rapp, J. Ailuno, A. P. Alloncle, P. Delaporte, *Optics express* **2011**, *19* (22), 21563 – 21574. DOI: 10.1364/OE.19.021563.
- [21] S. A. Mathews, R. C. Y. Auyeung, H. Kim, N. A. Charipar, A. Piqué, *Journal of Applied Physics* **2013**, *114* (6), 64910. DOI: 10.1063/1.4817494.
- [22] P. Sopenña, J. M. Fernández-Pradas, P. Serra, *Applied Surface Science* **2017**, *418*, 530 – 535. DOI: 10.1016/j.apsusc.2016.11.179.
- [23] F. Zacharatos, M. Makrygianni, I. Zergioti, *IEEE J. Select. Topics Quantum Electron.* **2021**, *27* (6), 1 – 8. DOI: 10.1109/JSTQE.2021.3084443.
- [24] M. Colina, M. Duocastella, J. M. Fernández-Pradas, P. Serra, J. L. Morenza, *Journal of Applied Physics* **2006**, *99* (8), 84909. DOI: 10.1063/1.2191569.
- [25] M. Duocastella, J. M. Fernández-Pradas, J. Domínguez, P. Serra, J. L. Morenza, *Appl. Phys. A* **2008**, *93* (4), 941 – 945. DOI: 10.1007/s00339-008-4741-6.
- [26] A. Palla-Papavlu, C. Córdoba, A. Patrascioiu, J. M. Fernández-Pradas, J. L. Morenza, P. Serra, *Appl. Phys. A* **2013**, *110* (4), 751 – 755. DOI: 10.1007/s00339-012-7279-6.